Heat Mass Transfer (2017) 53:591–609
DOI 10.1007/s00231-016-1843-0

ORIGINAL

Numerical study on heat and mass transfer in hygroscopic rotor during sorption process

Hyun-Geun Shin[1] · **Il Seouk Park**[1]

Received: 23 April 2015 / Accepted: 28 May 2016 / Published online: 2 June 2016

Abstract Recently, interest in hygroscopic dehumidifiers has rapidly increased in the indoor environment industry because of their potential contribution to the development of hybrid (refrigerating + hygroscopic) dehumidifiers. Heat and mass transport phenomena such as adsorption and desorption, and their complex interactions occur in a desiccant rotor, which comprises many small hygroscopic channels. This study numerically investigated the conjugated heat and mass transfers in a channel modeled with the flow and porous desiccant regions, where only ordinary and surface diffusions (excluding Knudsen diffusion) during the sorption processes were considered. The change in the dehumidification performance depending on operating conditions such as the rotor's rotating speed, air flow rate, and adsorption–desorption ratio, was examined under various working environments. The temporal and spatial variations in the temperature, vapor mass fraction, and liquid water mass fraction in the channel were considered in detail. The closely linked heat and mass transports were clarified for a better understanding of the sorption processes in the desiccant rotor.

List of symbols

$C_{p,d}$	Specific heat of desiccant at constant pressure
$C_{p,ha}$	Specific heat of humid air at constant pressure
$D_{o,ha}$	Ordinary diffusivity of humid air
$D_{s\_eff,d}$	Effective surface diffusivity
k_d	Thermal conductivity of desiccant
k_{ha}	Thermal conductivity of humid air
$h_{l,di}$	Enthalpy of liquid water at interface bordering desiccant layer
h_{ads}	Latent heat of water vapor
$h_{v,fi}$	Enthalpy of water vapor at interface bordering flow layer
$\dot{m}_{v,fi}$	Vapor mass flux at interface bordering flow layer
$\dot{m}_{\ell,di}$	Liquid water mass flux at interface bordering desiccant layer
p	Pressure
$\dot{q}_{ss}$	Heat flux of heat conduction at desiccant layer
$\dot{q}_{gs}$	Heat flux of heat conduction at flow layer
T	Temperature
t	Time
u	Velocity
x, y	Coordinate

Greek symbols

ρ_d^*	Apparent density of desiccant
ρ_{ha}	Density of humid air
ρ_l	Density of liquid water
φ_v	Vapor mass fraction (ratio of water vapor to humid air)
φ_l	Liquid water mass fraction (ratio of liquid water to desiccant)
ε_d	Porosity of desiccant layer
$\varepsilon_{d,dry}$	Porosity of desiccant layer under complete dry conditions

Subscripts

d	Desiccant
dry	Dry condition
eff	Effective
fg	Latent heat from phase change
g	Dry air
fi	Fluid layer at interface

✉ Il Seouk Park
einstein@knu.ac.kr

[1] School of Mechanical Engineering, Kyungpook National University, 80, Daehakro, Buk-gu, Daegu 702-701, Korea

i	Interface
l	Liquid water
p	Constant pressure
s	Surface diffusion
di	Desiccant layer at interface
v	Water vapor

Superscripts

*	Apparent

1 Introduction

There are two different dehumidification methods to lower indoor humidity by eliminating water vapor in the room air. The first is refrigerating dehumidification, which is based on the principle that water vapor condenses out of humid air when the temperature is lower than the dew point. In general, refrigerating dehumidification requires a vapor compression refrigerating device; thus, a large energy input is required to compress and circulate the refrigerant gas.

The other is hygroscopic dehumidification, which reduces the indoor humidity by adsorbing water vapor with a hygroscopic material. A general commercial hygroscopic dehumidifier adopts a hygroscopic rotor comprising many small channels made of hygroscopic materials. The channel is divided with two parts: the channel wall, which is called the desiccant layer, and the channel core region, which is the flow layer where the humid air passes through. The channel's hydraulic diameter is about several millimeters.

The rotor repeatedly takes in and expels water vapor while rotating. As the air passes through the rotor channel, the water vapor it contains is transferred to the rotor's hygroscopic wall (desiccant layer) and changes to liquid water in the desiccant layer. This vapor transport process is called adsorption. On the other hand, when hot or dry air passes through the channel, the water-holding capacity of the hygroscopic wall is significantly decreased under the resulting warm or highly dry conditions. Consequently, the water contained in the desiccant layer is expelled to the channel's flow region. This is the desorption process. The combined process of adsorption and desorption is called the sorption process [1–3].

The hygroscopic dehumidifier has very low energy consumption. However, the dehumidification capacity is lower than that of the refrigerating dehumidifier. To compensate for the weaknesses of both dehumidification methods and boost their strengths, studies of hybrid dehumidification combining refrigerating and hygroscopic dehumidification have actively been conducted [4, 5].

In the operation of a hygroscopic rotor, the heat and mass transfers by adsorption and desorption are closely interconnected. The dehumidification capacity is highly sensitive to the working environment, and is dramatically affected by operating conditions such as the adsorption-to-desorption ratio, rotor speed, and air mass flow rate. Therefore, to establish the right operating strategy for various working environments, a physical understanding of the changes in performance that are accompanied by the variations of the operating conditions and working environments is first required.

In a previous experimental study on hygroscopic rotors, Brillhart [6] considered the change in the sorption performance for various combinations of a porous desiccant and coated catalyst. Simonson et al. [7, 8] suggested a model for heat and mass transfer coefficients based on their experiments and conducted numerical simulations using this model. They assumed that the vapor adsorbed onto the desiccant is completely changed to liquid water at the interface between the flow and desiccant layers.

Such models for the heat and mass transfer coefficients have greatly contributed to simplifying numerical studies on the transport phenomena in the rotor. In other words, they have allowed the temporal and spatial changes in the desiccant's hygrothermal state to be evaluated by considering only the diffusion in the desiccant layer; the velocity, temperature, and humidity in the flow layer do not need to be solved [1, 9–12].

For a more simplified analysis, some numerical studies have adopted a lumped capacitance assumption in the direction of the desiccant's thickness [13, 14]. In these studies, the changes in the desiccant's temperature and humidity in the channel length direction were largely handled. Ruivo et al. [15, 16] proved that the lumped capacitance assumption is only available for a very thin desiccant layer: for heat transfer, it is applicable when the desiccant thickness is 5 mm or less; for mass transfer, it is applicable when the desiccant thickness is 0.1 mm or less. Also, they suggested that the properties' hygrothermal dependency should be reflected in the solution to improve the accuracy.

The mass diffusion in the hygroscopic channel is understood to be a combined process of the ordinary, surface, and Knudsen diffusions; however, ordinary diffusion can usually be neglected in porous desiccant structures having a small porosity. Many studies have been conducted to find out the dominant diffusion mechanism in various desiccant materials [1, 2, 9–11, 15, 17]. Pesaran [9] and Ruivo et al. [15] investigated the dominant diffusion mechanism in the silica gels RD and ID. They determined that the Knudsen diffusion is negligible in the silica gel RD, which has a very small pore size. Majumdar [10] introduced a concept for the effective diffusion coefficient that can explain the ordinary and Knudsen diffusions at the same time and investigated the sorption performance along with the composition ratio of the silica gel and catalyst. Dai et al. [11] solved the sorption phenomena using a single constant diffusion

coefficient without distinguishing between the diffusion mechanisms. Sphaier et al. [1] introduced a solution procedure that includes all three diffusion mechanisms. San et al. [17] solved the sorption problem by considering only the surface diffusion. They explained the sorption phenomenon with the heat transfer rate and heat capacitance rate.

In recent years, some research groups have solved the transport phenomena in the desiccant and flow layers simultaneously [3, 18, 19]. Fujii et al. [18] developed a solution procedure to conjugate the heat and mass transfers between the flow and desiccant layers and stressed the importance of the conjugation for the flow and desiccant layers through a comparison between the conjugate and non-conjugate results. In particular, they showed that the conjugate solution is absolutely necessary for cases with a thick desiccant layer. Hassan et al. [19] tried to apply turbulence effects in their conjugate transport problem and showed that the sorption was enhanced when the turbulence intensity was increased. Ruivo et al. [3] reported that conjugate analysis should be conducted for the cases with channel lengths of 10 cm or longer.

The effect of the cross-sectional shape of the channel composing the hygroscopic rotor has been investigated [14, 20–22]. Zhang et al. [14] and Sherony et al. [20] showed that a sinusoidal cross-section for the channel is the most effective for the sorption process in terms of the friction coefficient and Nusselt number. Gao et al. [21] explained that cross-sectional shapes such as the sinusoid or triangle, which have small interior angles, are more advantageous than other cross-sectional shapes with a larger interior angle. They also studied the sorption characteristics considering the rotor's rotating effect.

As noted earlier, the dehumidification performance of the hygroscopic rotor completely depends on the working environment and operating conditions. In hybrid dehumidifiers, the performance of the hygroscopic part can be greatly enhanced by regulating the operating conditions of the refrigerating part. Also, inversely, the operation results of the hygroscopic part affect the refrigerating part and overall dehumidification performance. Therefore, studying the dehumidifying characteristics under various working environments and operating conditions is very useful and essential.

In this study, we solved the two-dimensional and unsteady heat and mass transfer in a hygroscopic rotor that has been adopted for a hybrid dehumidifier that combines refrigerating and hygroscopic dehumidification. The desiccant layer is made of the silica gel RD. Thus, the Knudsen diffusion in the desiccant layer is negligible. The conjugate solutions for heat and mass transfers between the flow and desiccant layers were investigated. The variation in the dehumidification performance depending on rotor operating conditions such as the cycle period (rotor speed), desorption–adsorption time ratio, and air flow rate, was considered for various working environments. The temporal and spatial changes in the temperature, vapor mass fraction, and liquid water mass fraction in the flow and desiccant layers were examined.

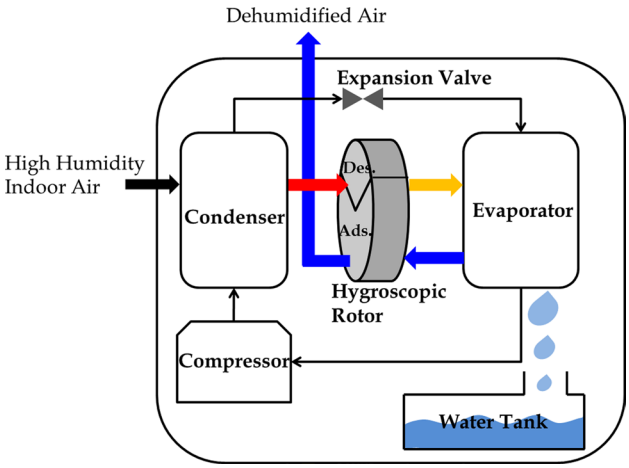

Fig. 1 Schematic of hybrid dehumidification

2 Mathematical and numerical modeling

A hybrid dehumidification system comprises a compression refrigerating dehumidification cycle and hygroscopic rotor. Figure 1 shows a schematic of the system. First, humid air enters the system. As the air passes through the condenser of the compression refrigerating part, it is heated by the heat released from the condenser. The heated humid air enters the desorption sector of the hygroscopic rotor and regenerates the rotor by desorbing the water vapor from the liquid water in the hygroscopic rotor. Thus, the air is highly humid just after it exits the desorption sector of the hygroscopic rotor; it then enters the evaporator of the compression refrigerating part. When the air passes through the evaporator, it cools down, and the water vapor in the air is condensed. The condensed liquid is drained to the reservoir tank. The cooled air exiting the evaporator contains a small amount of water vapor, but its low temperature means that the relative humidity is not pretty low. Next, the cooled air containing a small amount of water vapor passes through the adsorption sector of the hygroscopic rotor. The water vapor in the air adsorbs onto the rotor, and the dry air is finally supplied to the room.

2.1 Assumptions

In general, a hygroscopic rotor consists of many small channels, as shown in Fig. 2. We studied the heat and mass

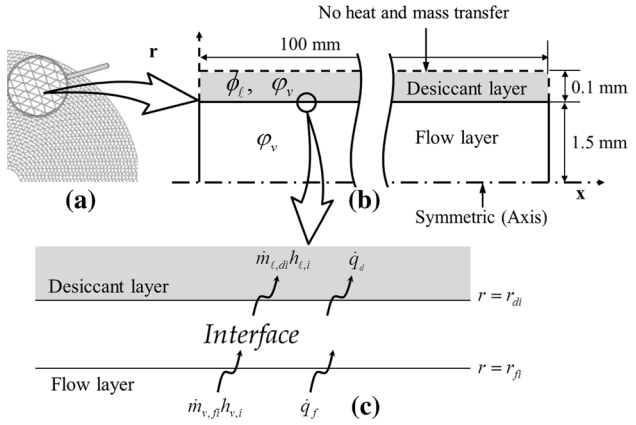

Fig. 2 Computational modeling of a single hygroscopic channel

Table 1 Properties of the desiccant layer

Porosity	0.485
Thermal conductivity	0.144 W/mK
Apparent density	1129 kg/m^3
Specific heat	921 J/kgK
Tortuosity	2.24

transfer phenomena in a single channel while neglecting the effect of the rotor's rotation. The channel was modeled as an axisymmetric circular tube consisting of a flow layer and desiccant layer, as shown in Fig. 2b. The desiccant layer is a thin porous barrier between neighboring channels. At the outer boundary of the channel on the desiccant layer, we assumed that there is no heat and mass transfer with neighboring channels.

The density and thermal conductivity of the desiccant layer was assumed to be constant. The liquid water and water vapor existing in the desiccant layer were exactly at hygrothermal equilibrium. The hygrothermal hysteresis of the material (i.e., the shift of the hygrothermal balance between the liquid and vapor phases by repeated sorption cycles under a given thermal condition) was neglected in this study. The study considered the silica gel RD as the hygroscopic material; for this gel, the Knudsen diffusion is less effective than the surface diffusion and thus can be neglected. The thermal and mass diffusions in the desiccant were assumed to be isotropic. Table 1 presents the information on the desiccant layer used in this study.

Air is forced into the dehumidifier by a blowing fan, so the humid air flow approaching the hygroscopic rotor is likely to be turbulent. However, the channel diameter was so small that the flow in the channel could be assumed to be laminar. As noted earlier, we neglected the rotor's rotating effect; thus, the incoming air only had an axial velocity component. Therefore, the radial and circumferential velocity components were neglected at the inlet of the channel.

2.2 Governing equations

Equations (1)–(4) are the conservation equations for mass, momentum, energy, and vapor mass fraction in the flow layer. Equations (5) and (6) are the conservation equations for energy and liquid water mass fraction in the desiccant layer. These conservation equations for the flow and desiccant layers were commonly used in previous studies [3, 15, 18, 19], that attempted to obtain conjugated solutions.

$$\frac{\partial \rho_{ha}}{\partial t} + \frac{\partial \left(\rho_{ha} u_j\right)}{\partial x_j} = 0 \tag{1}$$

$$\frac{\partial (\rho_{ha} u_i)}{\partial t} + \frac{\partial}{\partial x_j}\left(\rho_{ha} u_i u_j\right) = -\frac{\partial p}{\partial x_i} + \frac{\partial}{\partial x_j}\left(\mu_{ha}\frac{\partial u_i}{\partial x_j}\right) \tag{2}$$

$$\frac{\partial \left(\rho_{ha} C_{p,ha} T\right)}{\partial t} + \frac{\partial \left(\rho_{ha} C_{p,ha} u_j T\right)}{\partial x_j} = \frac{\partial}{\partial x_j}\left(k_{ha}\frac{\partial T}{\partial x_j}\right) \tag{3}$$

$$\frac{\partial (\rho_{ha}\varphi_v)}{\partial t} + \frac{\partial \left(\rho_{ha} u_j \varphi_v\right)}{\partial x_j} = \frac{\partial}{\partial x_j}\left(\rho_{ha} D_{o,ha}\frac{\partial \varphi_v}{\partial x_j}\right) \tag{4}$$

$$\frac{\partial \left(\rho_d^* C_{p,d} T\right)}{\partial t} = \frac{\partial}{\partial x_j}\left(k_d \frac{\partial T}{\partial x_j}\right) + \frac{\partial}{\partial t}\left(-\rho_{ha,d}^* \varphi_v h_{ads}\right) \tag{5}$$

$$\frac{\partial \left(\rho_d^* \varphi_l\right)}{\partial t} = \frac{\partial}{\partial x_j}\left(\rho_d^* D_{s\_eff,d}\frac{\partial \varphi_l}{\partial x_j}\right) - \frac{\partial \left(\rho_{ha,d}^* \varphi_v\right)}{\partial t} \tag{6}$$

The subscripts *ha* and *d* represent the humid air and desiccant, respectively. The superscript * represents the apparent value. The u_j is the velocity vector, p is the pressure, T is the temperature, φ_v is the mass fraction of the water vapor to the humid air, and φ_l is the mass fraction of the liquid water to the solid desiccant. The ρ is the density, μ is the dynamic viscosity, k is the thermal conductivity, C_p is the specific heat at constant pressure, and D is the diffusion coefficient.

The last terms on the right-hand sides of Eqs. (5) and (6) show the heat and mass source (or sink) by the sorption process. The increase or decrease in the amount of liquid water in the desiccant layer by the sorption process is reflected as a mass source in Eq. (6), and the corresponding sorption heat is applied as a heat source in Eq. (5) for the desiccant layer. The h_{ads} is the sum of the latent heat of vaporization and heat of wetting; this can be expressed by Eq. (7) [3].

$$h_{ads} = -0.02T^3 + T^2 - 2386.2T + 2501600 + 1000 \times (420\varphi_l - 375.867 - 550\log\varphi_l) \quad (7)$$

The ordinary diffusivity of the water vapor to humid air in the flow layer $D_{o,ha}$ can be presented as a function of the temperature and pressure, as given in Eq. (8) [9].

$$D_{o,ha} = 1.758 \times 10^{-4} \frac{(T + 273.15)^{1.685}}{P} \quad (8)$$

The effective surface diffusivity of the liquid water in the desiccant layer $D_{s\_eff,d}$ is a function of the temperature and tortuosity τ, as given in Eq. (9), because the surface diffusion is relevant to the diffusion path [15].

$$D_{s\_eff,d} = \frac{1.6 \times 10^{-6}}{\tau} \exp\left[-0.974 \times 10^{-3} \times \frac{h_{ads}}{T + 273.15}\right] \quad (9)$$

The apparent density of humid air in the desiccant layer $\rho^*_{ha,d}$, as presented in Eqs. (5) and (6), can be calculated with Eq. (10) by using the porosity of the desiccant layer ε_d and density of humid air in the flow layer ρ_{ha}.

$$\rho^*_{ha,d} = \varepsilon_d \rho_{ha} \quad (10)$$

The porosity of the desiccant layer ε_d can be expressed by Eq. (11):

$$\varepsilon_d = \varepsilon_{d,dry} - \varphi_l \frac{\rho^*_d}{\rho_l} \quad (11)$$

where $\varepsilon_{d,dry}$ is the porosity of the desiccant layer under completely dry conditions and ρ^*_d is the apparent density of the desiccant layer. This is determined by considering the original density of the desiccant material and the porosity of the desiccant layer. The ρ_l is the density of the liquid water in the desiccant layer.

2.3 Boundary conditions and conjugate method at interface between flow and desiccant layers

As noted earlier, the channel was assumed to be axisymmetric with no heat and mass transfer between neighboring channels. For the momentum, the no-slip boundary condition is applied at all wall boundaries, including the interface between the flow and desiccant layers.

$$u = 0 \text{ (at all walls)} \quad (12)$$

At the inlet, a uniform normal velocity condition is applied, while the other components of the velocity are set to zero.

$$u_x = V_{in}, \quad u_r = u_\theta = 0 \text{ (at inlet)} \quad (13)$$

At the outlet, the normal derivative of the velocity is zero.

$$\frac{\partial u_i}{\partial x} = 0 \text{ (at outlet)} \quad (14)$$

For the temperature and mass fractions of the water vapor and liquid water, the conditions of a constant temperature and mass fraction are applied at the inlet.

$$\mathcal{T} = \mathcal{T}_{in}, \quad \varphi_v = \varphi_{v,in} \text{ (at inlet)}, \quad \varphi_l = \varphi_{l,in} \quad (15)$$

The zero normal derivative conditions are applied at the outlet for the temperature and mass fractions.

$$\frac{\partial T}{\partial x} = \frac{\partial \varphi_v}{\partial x} = \frac{\partial \varphi_l}{\partial x} = 0 \text{ (at outlet)} \quad (16)$$

In this study, we solved the *advection* of the *water vapor* in the flow layer, whereas we only solved the *diffusion* of the *liquid water* in the desiccant layer. Thus, a slightly complex conjugating procedure between the flow and desiccant layers was applied at the interface. First, we assumed that the vapor mass flux at the interface bordering the flow layer $\dot{m}_{v,fi}$, which is the mass flux of the water vapor transported from the flow layer to the desiccant layer, is equal to the liquid water's mass flux at the interface bordering the desiccant layer $\dot{m}_{l,di}$. This is given in Eq. (17) [15].

$$\dot{m}_{v,fi}\left(= \frac{-\rho_{gv} D_{o,ha}}{1 - \varphi_{v,fi}} \left.\frac{\partial \varphi_v}{\partial r}\right|_{r=r_{fi}}\right) = \dot{m}_{l,di}\left(= -\rho^*_d D_{s\_eff,d} \left.\frac{\partial \varphi_l}{\partial r}\right|_{r=r_{di}}\right) \quad (17)$$

In reality, the vapor transported from the flow layer affects changes in both water vapor and liquid water present in the desiccant layer. However, the hygroscopic material used in this study was the silica gel RD, which is known to have negligible Knudsen diffusion and be very thermally sensitive to changes in the hygrothermal condition. We assumed that the vapor transported from the flow layer first changes in phase to a liquid, and then diffuses into the desiccant layer by surface diffusion.

The vapor mass fraction in the desiccant layer is calculated from the liquid water mass fraction and the following hygrothermal equilibrium condition given in Eq. (18) [3]:

$$\varphi_v = \frac{\psi p_{sat}}{\psi p_{sat} + (p - \psi p_{sat}) R_v / R_a} \quad (18)$$

$$\psi = 1.0132 - \sqrt{1.0265 - 2.632\varphi_l} \quad (19)$$

where R_v and R_a are the gas constants for the water vapor and air, respectively, in the desiccant layer and p_{sat} is the saturated vapor pressure at a given temperature.

The vapor mass fraction $\varphi_{v,di}$ at the interface bordering the desiccant layer, which is calculated by Eq. (18), should

be equal to the vapor mass fraction $\varphi_{v,fi}$ at the interface bordering the flow layer. To conjugate the vapor transport in both layers, we perform a numerical iteration until the continuities for the vapor mass fraction and transported mass flux at the interface are satisfied.

When solving Eq. (4) in the flow layer, we first apply the Dirichlet boundary condition at the interface by using the vapor mass fraction that is calculated from the hygrothermal equilibrium of Eq. (18) in the desiccant layer. When solving the liquid water mass fraction of Eq. (6) in the desiccant layer, we apply the Neumann boundary condition at the interface. That is, at the interface, the normal derivative of the liquid water mass fraction is substituted by using the vapor mass flux at the interface bordering the flow layer, which is obtained as a solution to Eq. (4) in the flow layer; this is described in Eq. (17). Next, both regions are iteratively calculated until the vapor mass fractions at the interfaces bordering the flow and desiccant layers converge within a specific error range.

Equation (20) shows the heat balance at the interface between the flow and desiccant layers. The $h_{v,fi}$ is the enthalpy of the transported water vapor at the interface bordering the flow layer, and $h_{l,di}$ is the enthalpy of the liquid water at the interface bordering the desiccant layer. Equation (20) represents the energy balance between the enthalpy exchanges of the transported mass and conductive heat transfer [15]. Figure 2c shows a conceptual sketch of the energy balance in the infinitesimally small control volume, which includes the interface.

$$\dot{m}_{v,fi}h_{v,fi} + \dot{q}_{fi} = \dot{m}_{l,di}h_{l,di} + \dot{q}_{di} \tag{20}$$

The $\dot{q}_{fi}\left(= -k_{ha}\,dT/dr\big|_{at\ interface}\right)$ and $\dot{q}_{di}(= -k_d dT/dr|_{at\ interface})$ are the conductive heat fluxes calculated at the interfaces bordering the flow and desiccant layers, respectively. The k_{ha} is the thermal conductivity of the humid air in the flow layer. The k_d is the thermal conductivity of the solid desiccant.

For the thermal field, the temperature and heat flux at the interface should be continuous, similar to the mass fraction. Therefore, to forcibly conjugate the thermal fields in both the flow and desiccant layers, we first solve Eq. (5) in the desiccant region by using the Dirichlet boundary condition at the interface. The interface temperature, which is used as a boundary condition, is obtained from the solution of Eq. (3). Next, the interface heat flux $\dot{q}_{di}$ in the desiccant layer, which is obtained from the solution of Eq. (5), and the heat balance constraint at the interface of Eq. (20) are used to set the diffusive heat flux at the interface bordering the flow layer. Then, Eq. (3) is solved in the flow layer. The iteration continues until the interface temperatures calculated in both flow and desiccant layers converge within a specific error range.

3 Results and discussions

3.1 Validation

Before getting into the heat and mass transfer characteristics inside the hygroscopic rotor under various operating conditions, the validation procedures for the numerical modeling employed in this study were preceded. In the other words, the validity of the present conjugating method for heat and mass transfers and the selected governing equation set was investigated. We selected Zhang et al. [2] and Ruivo et al. [3] works as verification problems.

Zhang et al. [2] validated their simple numerical model by comparing simulation results with experimental ones. There are distinct features between their model and ours. First, their numerical model dealt with the dependent variables such as temperature and humidity only in desiccant layer whereas our model is more precise by calculating the heat and mass transfer not only in solid desiccant but also in fluid zone. In addition, they neglected heat and mass diffusions along the flow direction. Figure 3 shows the temperature changes at the channel exit at the end of each consecutive cycle. As shown in the figure, the result of our model shows better agreement with the experiment than their numerical model which neglected the heat and mass transfer in the channel flow region. The details of the calculating condition were well described in Ref. [2].

The Ruivo's problem is the transient adsorption process in a circular hygroscopic channel with a length of 10 cm, inner radius of 1.5 mm, and desiccant layer thickness of 0.1 mm. The initial temperature of the channel was 100 °C. The initial liquid water mass fraction (φ_l) in the desiccant layer was 0.012, and its corresponding hygrothermal equilibrium vapor mass fraction (φ_v) was 0.0098. This vapor mass fraction of 0.0098 was also set as the initial condition

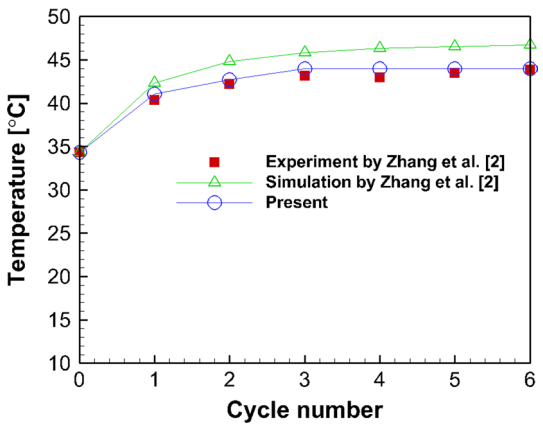

Fig. 3 Comparison of vapor temperature with Zhang et al.'s results [2]

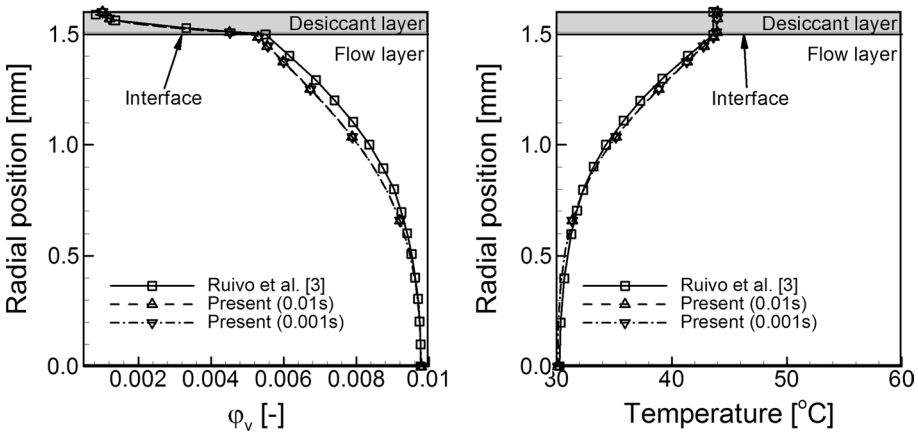

Fig. 4 Comparison of vapor mass fraction and temperature with Ruivo et al.'s results [3] (X = 7.6 mm, t = 10 s)

for the vapor mass fraction in the flow layer. The temperature and vapor mass fraction (φ_v) of the inflowing humid air were 30 °C and 0.01, respectively. The mass flux of the inflowing air was 1.5 kg/m^{2}s (i.e., the mass flow rate for a single channel was 1.06×10^{-5} kg/s).

Figure 4 shows the profiles of the vapor mass fraction and temperature in the cross-section at x = 7.6 mm (at 7.6 mm from the channel inlet in the axial direction) at 10 s after the initial state. A grid system of 50 (axial) × 36 (radial) nodes was applied. Ten grid nodes in the radial direction were allocated to the desiccant layer of 0.1 mm thickness. To check the time-step dependency, time steps of 0.1, 0.01, and 0.001 s were tested. However, we could not obtain a converged solution with the time step of 0.1 s. As shown in the figure, no time-step dependency was detected for time steps of 0.01 s or less. Thus, we applied the time step of 0.01 s in all further simulations.

As shown in Fig. 4, although the water vapor was transported from the flow layer to the desiccant layer by the difference in the vapor mass fractions between the inflowing air ($\varphi_v = 0.01$) and initial desiccant ($\varphi_v = 0.0098$), the vapor mass fraction in the desiccant ($\varphi_v = 0.0015 - 0.006$) was significantly reduced from the initial value of 0.0098. This is because the vapor remaining in the pore structure of the desiccant layer was abruptly adsorbed onto the hygroscopic material and condensed there because of the lowered temperature of the desiccant, which quickly responded to the cooling effect of the cold inflowing air of 30 °C. That is, the desiccant first responds to the very low temperature (30 °C) of the incoming air, so its ability to hold liquid water in its hygroscopic material abruptly increases; therefore, the water vapor initially presented in the desiccant pore is rapidly liquefied into the hygroscopic material. As a result, in the early stage, the vapor mass fraction in the desiccant is significantly reduced and the liquid water mass fraction correspondingly increases.

As shown in Fig. 4, boundary layers for the vapor mass fraction and temperature were observed in the flow layer. In the desiccant layer, an almost linear distribution of the vapor mass fraction was produced, whereas the temperature was nearly uniform. This is because thermal diffusion is much faster and stronger than mass diffusion in the present desiccant material (i.e., silica gel RD). The temperature in the desiccant was expected to gradually change to the temperature of the inflowing humid air of 30 °C. The present numerical model with a grid system of 50 (axial) × 36 (radial) and a time step size of 0.01 s reproduced Ruivo et al.'s results quite well.

3.2 Transient behaviors of heat and mass transfer in channel

To observe the heat and mass transfer characteristics in the channel during the repeated adsorption and desorption processes, we conducted a transient simulation for 30 cycles of desorption and adsorption with a cycle period of 60 s and desorption–adsorption time period ratio (D–A ratio) of 5–5, i.e., desorption for the first 30 s and adsorption for the last 30 s. The material and dimensions of the channel were the same as those used for the verification problem presented in Fig. 4. Initially, the temperature of the channel was 10 °C, the liquid water mass fraction in the desiccant layer (φ_l) was 0.185, and the equilibrium vapor mass fraction (φ_v) was 0.0021. Table 2 lists the operating conditions used for the present computation.

First, during the desorption stage of 30 s, hot humid air flowed into the channel from the left side with a temperature of 40 °C, vapor mass fraction (φ_v) of 0.01, and mass flow rate of 0.02 kg/s (this mass flow rate was calculated based on the entire rotor with a radius of 0.1 m and D–A ratio of 5–5; the recalculated mass flow rate for a single channel was 0.9×10^{-5} kg/s). For the next 30 s of the adsorption stage, cold dry air flowed into the channel from the right side with a temperature of 10 °C, a vapor mass fraction (φ_v) of 0.004, and the same mass flow rate (0.02 kg/s) as that for the desorption process.

Table 2 Parameters for computation

Initial condition	
Temperature	10 °C
Liquid water mass fraction	0.185
Inlet condition	
Adsorption	
Mass flow rate of humid air	0.02, 0.03, 0.04 kg/s
Temperature	10 °C
Vapor mass fraction	0.004
Desorption	
Mass flow rate of humid air	0.02, 0.03, 0.04 kg/s
Temperature	40 °C
Vapor mass fraction	0.01 (RH = 20 %), 0.02 (RH = 40 %), 0.03 (RH = 60 %)
Channel geometry	
Radius for flow layer	1.5 mm
Desiccant layer thickness	0.1 mm
Channel length	100 mm
Period of cycle	60, 120, 240, 360, 480, 540, 1200, 1800 s
D–A ratio	2–8, 3–7, 5–5, 7–3, 8–2

Figure 5 shows the changes in the isotherms in the channel over time. The channel temperature very rapidly changed to the temperature of the inflowing humid air. In the desiccant layer ($r \geq 1.5$ mm), the temperature was nearly uniform in the radial direction because of the thin thickness of the desiccant region and its strong thermal diffusion characteristics. First, during the desorption period in the initial 30 s, 40 °C humid air enters from the left side. The channel and desiccant were initially at 10 °C. The channel warms rapidly, starting from the channel core region, and reaches an average temperature of about 35 °C at 5 s. Next, during the adsorption period in the next 30 s, air at 10 °C enters from the right side. As shown in Fig. 5, the temperature of the entire channel is about 40 °C at the end of desorption period (t = 30 s). Because cold air at 10 °C enters from the right side, the channel is rapidly cooled. As shown in the figure, the average temperature of the channel reaches about 16 °C at 5 s after the beginning of the adsorption period ($t = 35$ s).

Figure 6 shows the temperature profiles in the channel at the corresponding times (2, 5, 30, 32, 35, and 60 s). The temperature data were extracted from the mid-position in the channel length direction, i.e., x = 5 cm. As shown in Fig. 5, the temperature in the channel developed very rapidly and became almost uniform throughout the channel. The initial channel temperature was 10 °C. Five seconds after the hot air starts to be supplied, the minimum and maximum temperatures in the channel are about 32 and 38 °C, respectively. That is, the channel is rapidly heated and has a quite uniform thermal distribution. These thermal characteristics appear again in the adsorption process from 30 to 60 s. In hybrid dehumidifiers, the channel is repeatedly heated and cooled down through desorption and adsorption cycle. However, this is not caused by endothermic or exothermic phenomena during the sorption processes but largely by the thermal condition of the inflowing humid air. That is, the dehumidification performance of the hygroscopic rotor can be changed by the inflowing air conditions, which are largely determined by the operation of the refrigerating part. In other words, the hybrid effect can be maximized by regulating the operating conditions of the compression refrigerating part, such as the operating temperatures of the condenser and evaporator and the refrigerant circulating flow rate.

Figure 7 shows the distribution of the vapor mass fraction (φ_v) in the channel over time. Early in the desorption process (from 0 to 5 s), the vapor mass fraction in the flow layer ($r < 1.5$ mm) was greater than that in the desiccant layer. However, in the last stage of the desorption period (from 5 to 30 s), the vapor mass fraction in the desiccant layer was greater than that in the flow layer. In the early stage, the incoming humid air ($\varphi_v = 0.01$) had a larger vapor mass fraction than the air ($\varphi_v = 0.0021$) remaining in the desiccant layer. Therefore, firstly the water vapor in the inflowing humid air was transported to the desiccant, so the vapor mass fraction in the desiccant layer started to increase in the early desorption stage. In actuality, the amount of the liquid water in the desiccant also slightly increased during the early desorption stage even as the desorption process proceeded; this will be presented in Fig. 11. During this period, the desiccant's thermal state rapidly developed under a new thermal condition caused by the air inflow, as shown in Figs. 5 and 6. Even after this short rapid transition period (from 0 to 5 s), the desiccant's

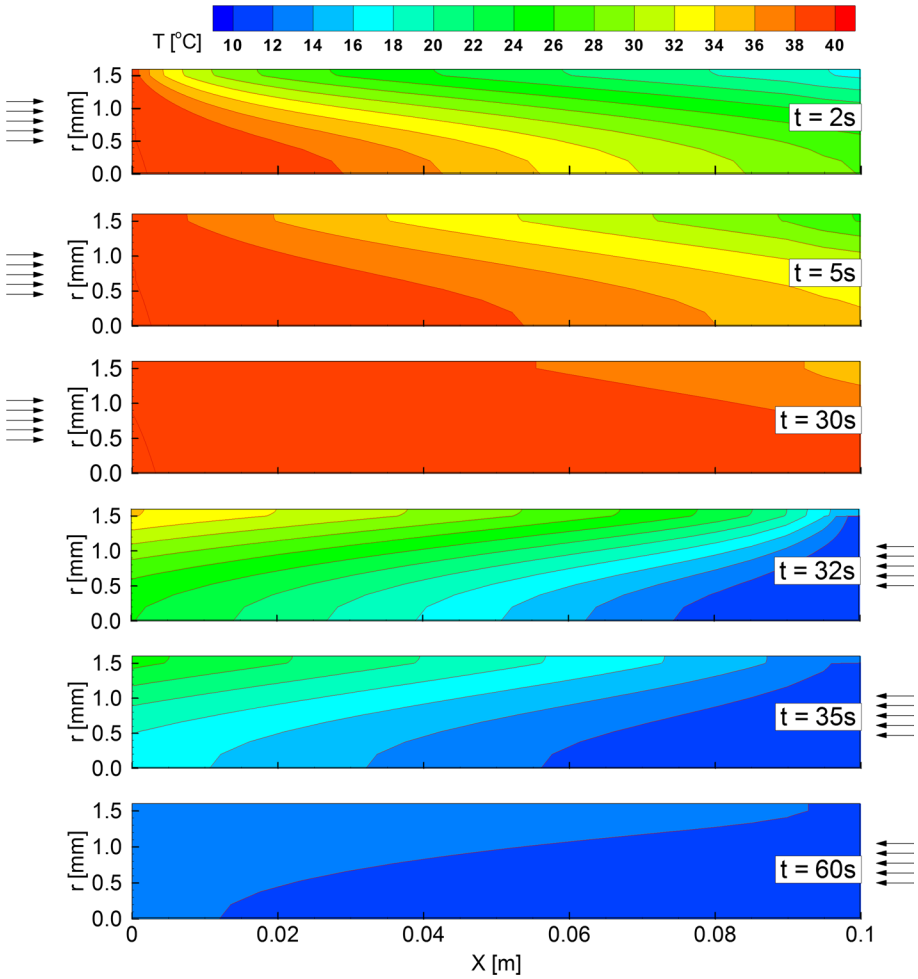

Fig. 5 Progression of isotherms in channel during one steady cycle (relative humidity of air = 20 %, D–A ratio = 5–5, air flow rate = 0.02 kg/s, and cycle period = 60 s)

thermal state was developed continuously by the supplied air. During this continuous and slow change in the desiccant's thermal state, water vapor was expelled from the desiccant pore structure to make a hygroscopic balance in the changed thermal state. Thus, as shown at 30 s in Fig. 7, the desiccant has a larger vapor mass fraction than the flow layer after this short transition period (0–5 s).

Similar to the desorption process, in the adsorption process (from 30 to 60 s) in Fig. 7, the transient changes of the vapor mass fraction in the channel were observed. In the early stage of the adsorption process (from 30 to 35 s), the vapor in the desiccant is transported to the flow region even as the adsorption process proceeds, because the cold and very dry air (10 °C, $\varphi_v = 0.004$) enters the channel. First, the desiccant is quickly cooled by the supplied cold air. During this early adsorption period (30 to 35 s), owing to the imbalance of the vapor mass fraction between the supplied air and the air present in the desiccant layer, vapor is transferred from the desiccant to the flow layer. Therefore, the amount of liquid water in desiccant decreases slightly during this early adsorption stage. After this period of rapid thermal development (cooling), the desiccant is still thermally being developed by the supplied cold air and adsorbs vapor from the supplied air to reach a new hygrothermal balance matching the incoming air's thermo-psychrometric conditions. Thus, the desiccant has a lower vapor mass fraction than the flow layer and starts to perform its adsorption function.

All of these transient behaviors were caused by the hygrothermal imbalance between the desiccant and inflowing humid air. In other words, excessively cold and dry (for desorption period, excessively hot and humid) air entered the channel compared to the present desiccant's temperature and vapor mass fraction. For better understanding, Fig. 8 shows the vapor mass fraction profiles at the mid-position in the length direction of x = 5 cm over time. If the channel's hygrothermal change becomes stable after it passes through the quick transient periods in the early desorption and adsorption processes, only very small differences in the vapor mass fraction between the desiccant and flow layers are formed across the channel as shown at 30 and 60 s in Fig. 8. In addition, the vapor mass fraction in the desiccant is clearly smaller (larger) than that in the flow layer in the early desorption (adsorption) period but

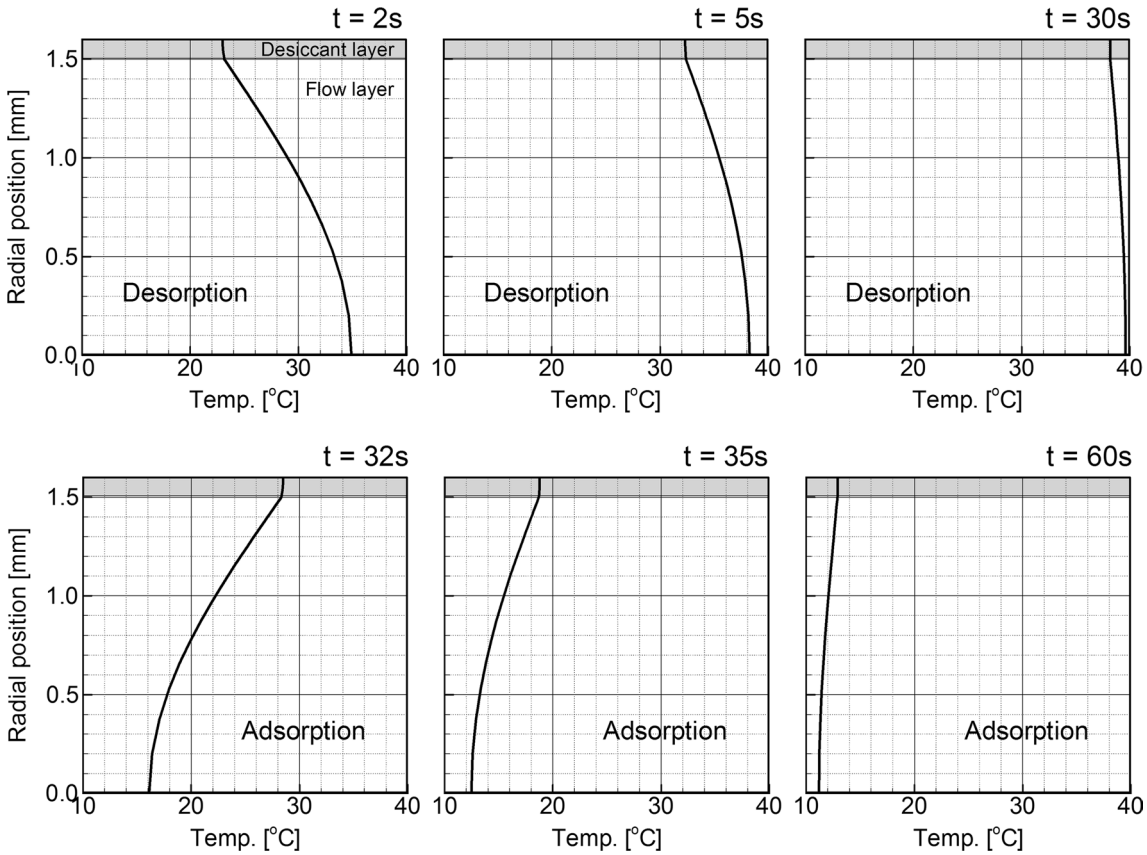

Fig. 6 Progression of temperature profile at x = 5 cm in channel (relative humidity of air = 20 %, D–A ratio = 5–5, air flow rate = 0.02 kg/s, and cycle period = 60 s)

becomes larger (smaller) than that in the flow layer after the initial 5 s. Anyway, by the present conjugate heat and mass transfer analysis, the details of the vapor transport phenomena could be revealed in both the flow and desiccant layers.

Figure 9 shows the changes in the temperature, vapor mass fraction (φ_v), and liquid water mass fraction (φ_l) in the desiccant as the cycle repeated. The values in Fig. 9 were averaged by volume weight for the entire desiccant layer. The changes in the temperature and vapor mass fraction were almost periodic from the initial stage. Their upper and lower values were approximately those of the inflowing humid air during the desorption and adsorption processes, respectively. In contrast, the ranges of the upper and lower values for the liquid water mass fraction continuously decreased until the seventh or eighth cycle. Then, the liquid water mass fraction reached a steady-periodic state. This is evidence that the present initial hygrothermal state of the desiccant (10 °C, $\varphi_v = 0.0021$, and $\varphi_l = 0.185$) is much wetter than the incoming air's thermo-psychrometric conditions (40 °C, $\varphi_v = 0.01$ for desorption and 10 °C, $\varphi_v = 0.004$ for adsorption). Of course, if the initial hygrothermal state of the desiccant is much drier than the present case, the liquid water mass fraction in Fig. 9c can show an increasing pattern. Further, this means that the hygroscopic development is much slower than the thermal development in the present hygroscopic material, and the desiccant-type dehumidifier can show completely different performances under the different thermal conditions. Also technically it means that under the various air conditions the hygroscopic rotor could be operated to maximize its performance by regulating the thermal conditions of supplied air.

Figure 10 maps the traveling course of the desiccant's hygrothermal state. The vertical and horizontal axes represent the liquid water mass fraction and vapor mass fraction, respectively. For better understanding, the constant temperature lines are depicted together. The hygrothermal state in the desiccant started to change from the initial condition of 10 °C, φ_v of 0.0021 and φ_l of 0.185. In the first 30 s of the desorption process, the desiccant's temperature and vapor mass fraction rapidly increased for the first 5 s because of the entering of the hot and humid air of 40 °C and $\varphi_v = 0.01$. As noted earlier in Figs. 7 and 8, the liquid water mass fraction slightly increased for the first 5 s: as the desiccant was rapidly heated in this early stage and the vapor in the inflowing air was rapidly transported

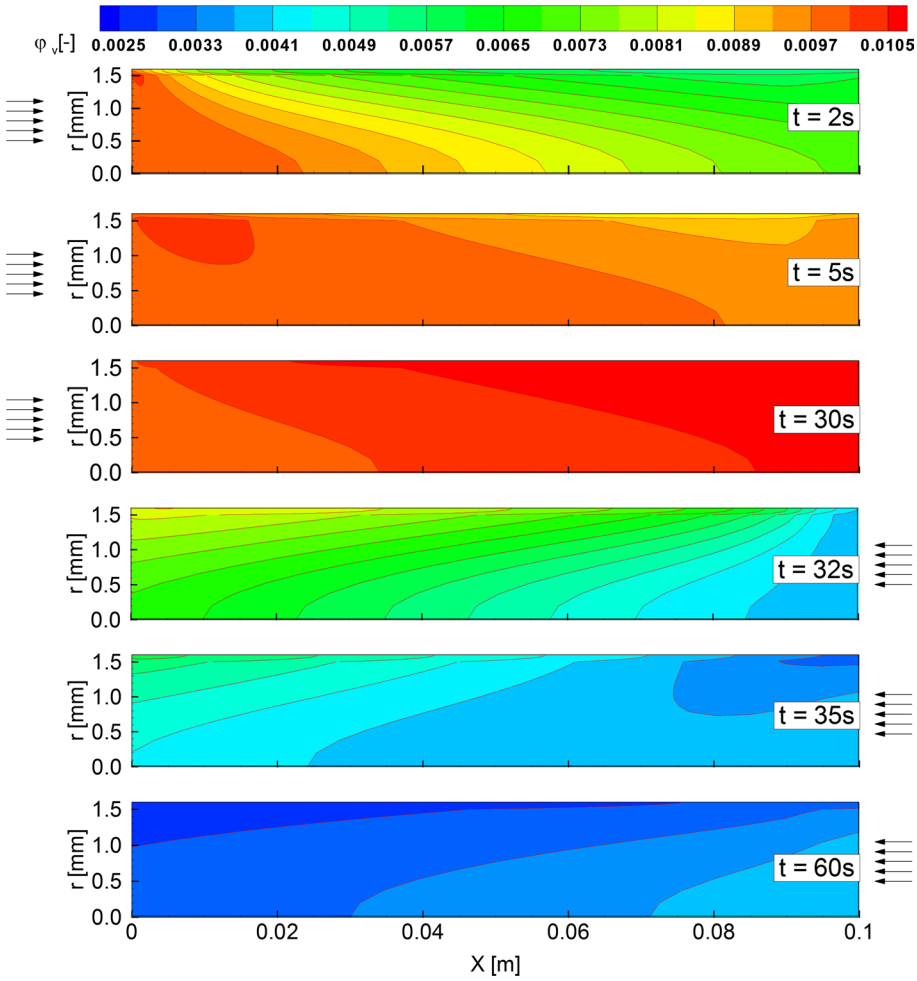

Fig. 7 Progression of vapor mass fraction in channel during one steady cycle (relative humidity of air = 20 %, D–A ratio = 5–5, air flow rate = 0.02 kg/s, and cycle period = 60 s)

from the flow layer to the desiccant layer, the desiccant arrived at a new hygrothermal balance corresponding to its changed temperature and vapor mass fraction by adjusting its liquid water content. Thus, during this early desorption period (0–5 s), the temperature and vapor mass fraction in the desiccant increased rapidly and significantly, and the liquid water mass fraction increased slowly and slightly. Because hot air at 40 °C entered, the heated hygroscopic material originally had a low capacity to contain liquid water. In the present early desorption period, however, the abrupt increase in the vapor mass fraction in the desiccant is caused not by the desiccant's vapor discharge but by vapor mass transfer from the flow layer to the desiccant layer due to the introduction of highly humid air. This vapor mass transfer from the flow layer forces the vapor in the desiccant pore structure to be liquefied into the desiccant. Thus, in this early desorption period, the liquid mass fraction increases slightly.

From around 5 s, the actual desorption started, and the liquid water mass fraction started to decrease. During the period of 5–30 s, the changes in the temperature and vapor mass fraction became very slow, and the liquid water mass fraction in the desiccant dropped significantly because of vapor mass transfer from the desiccant to the flow layer due to the spatial gradient of the vapor mass transfer between the flow and desiccant layers, as shown in Figs. 7 and 8. Because the desiccant arrives at a type of hygrothermal inflection point at around 5 s, the vapor mass fraction in the desiccant layer becomes greater than that in the flow layer, and heating of the desiccant by the hot inflowing air causes the hygroscopic material to expel water vapor. Further, the water vapor expelled from the desiccant's hygroscopic material is transferred to the flow layer.

During the adsorption period of 30–60 s, similar patterns of hygrothermal change were repeated. During the early adsorption process from 30 to 36 s, the desiccant's temperature and vapor mass fraction rapidly decreased; on the other hand, the desiccant's liquid water mass fraction decreased slightly as the desiccant sought a new hygrothermal balance. Similarly, the rapid decrease in the vapor mass fraction in the desiccant is caused not by the desiccant's vapor adsorption by cooling due to the cold inflowing air but by vapor transfer from the desiccant

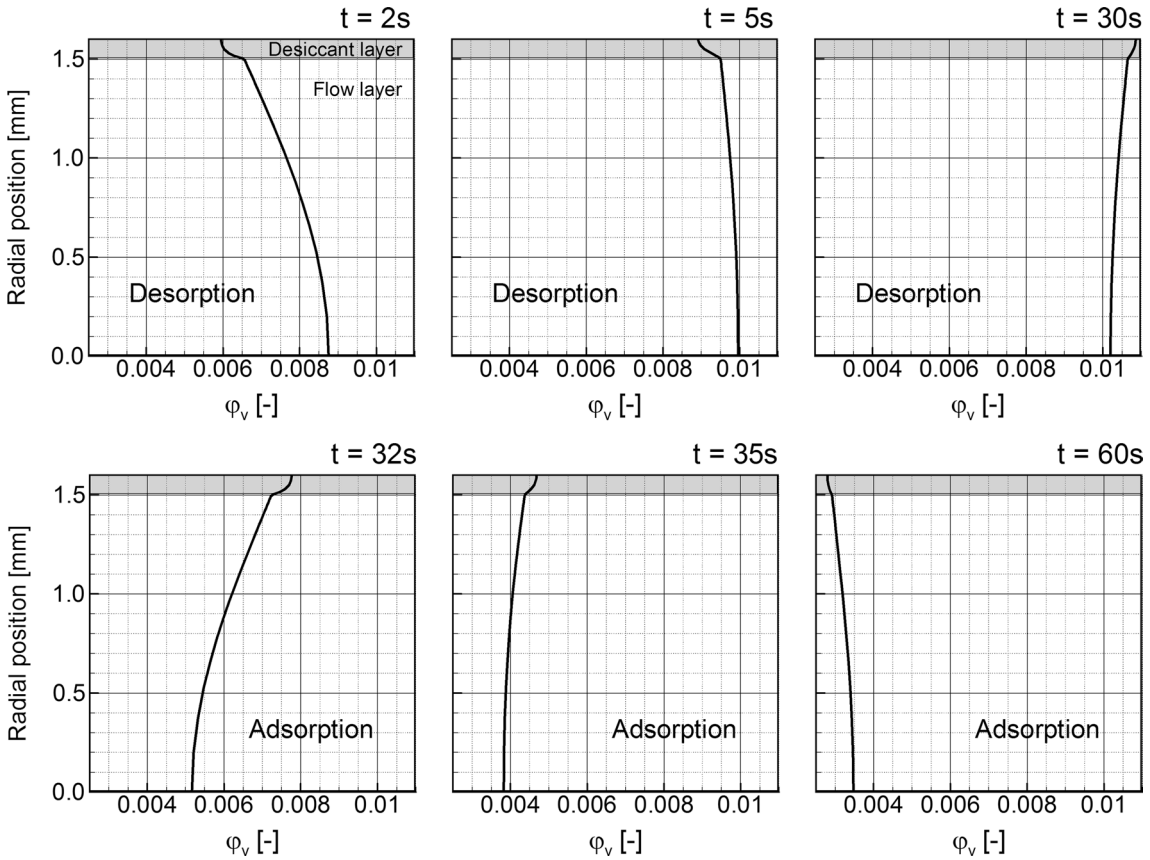

Fig. 8 Progression of vapor mass fraction profile at x = 5 cm in channel (relative humidity of air = 20 %, D–A ratio = 5–5, air flow rate = 0.02 kg/s, and cycle period = 60 s)

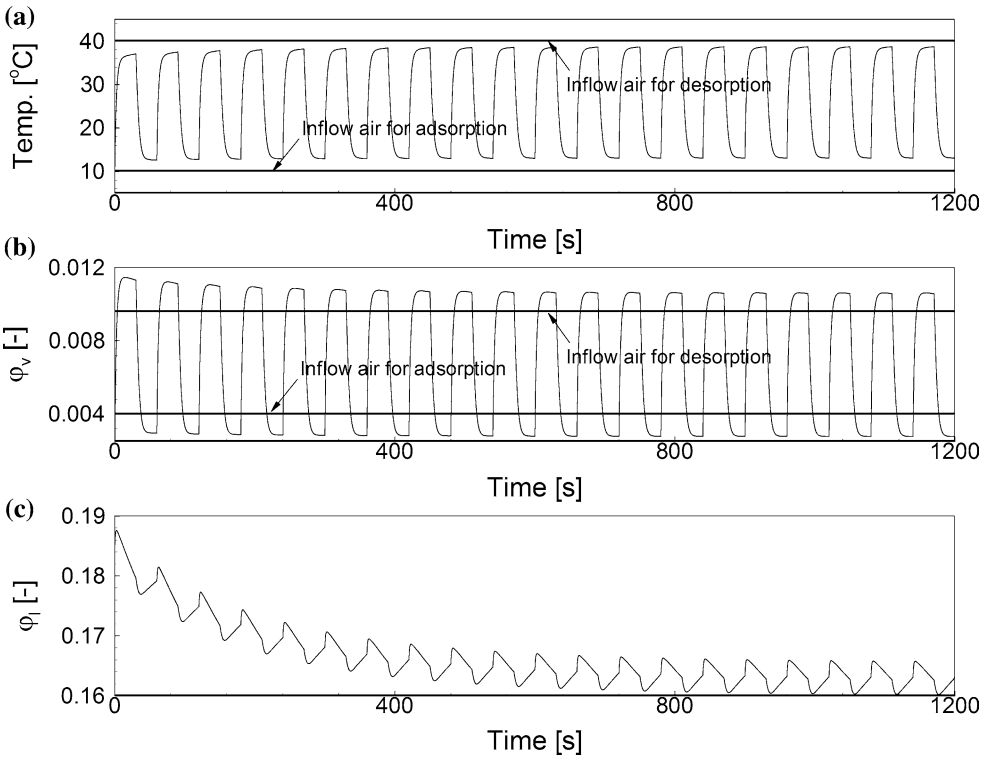

Fig. 9 Transient variations in **a** temperature, **b** vapor mass fraction, and **c** water mass fraction in desiccant layer (relative humidity of air = 20 %, D–A ratio = 5–5, air flow rate = 0.02 kg/s, and cycle period = 60 s)

layer to the flow layer due to the introduction of highly dry air.

For the next 24 s (from 36 to 60 s) after a hygrothermal inflection point was reached, small drops in the temperature and vapor mass fraction were observed, and the liquid water mass fraction was significantly increased by vapor mass transfer from the flow to the desiccant layer. Of course, vapor transfer from the flow to the desiccant layer occurs because the desiccant's water holding capacity is boosted as the desiccant is cooled by the cold inflowing air after the hygrothermal inflection point.

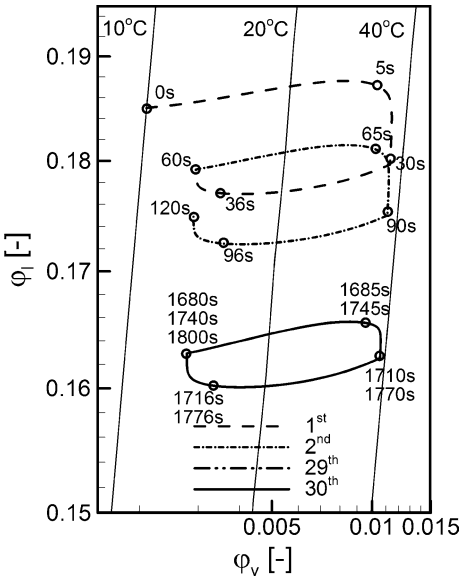

Fig. 10 Tracking of desiccant's hygrothermal state during consecutive sorption cycles (relative humidity of air = 20 %, D–A ratio = 5–5, air flow rate = 0.02 kg/s, and cycle period = 60 s)

In the early cycles (0–60 s and 60–120 s), the desiccant's hygrothermal state constantly changed with each cycle because of a large gap between its initial hygrothermal condition and the inflowing air's thermo-psychrometric condition. After several cycles passed, the desiccant's hygrothermal cycle exhibited a steady behavior, as shown in Fig. 10. Thus, the 29th (1680–1740 s) and 30th (1740–1800 s) cycles completely overlapped. By the transient conjugated heat and mass transfer analysis in both regions for several consecutive cycles, the increase or decrease of the vapor and liquid mass fraction during the cycle could be physically explained in this study.

Figure 11 presents the time variations in the averaged liquid water mass fraction and averaged temperature in the desiccant layer during a single steady cycle. Figures 11a, b show that the hygrothermal surge phenomena in the early stages of desorption and adsorption were closely connected with the thermally developing process in the desiccant. The amount of dehumidified water for one cycle can be estimated from Fig. 11a. The difference in liquid water mass fractions between the ends of the desorption and adsorption can be regarded as the amount of dehumidified water for one cycle. The present case favored a dehumidifying

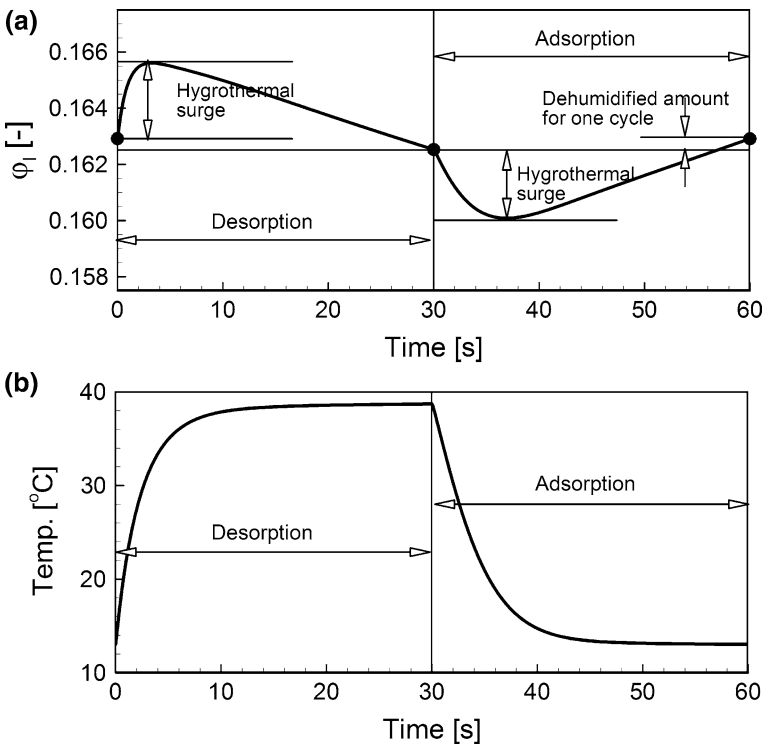

Fig. 11 Changes in **a** water mass fraction and **b** temperature in desiccant during single steady cycle (relative humidity of air = 20 %, D–A ratio = 5–5, air flow rate = 0.02 kg/s, and cycle period = 60 s)

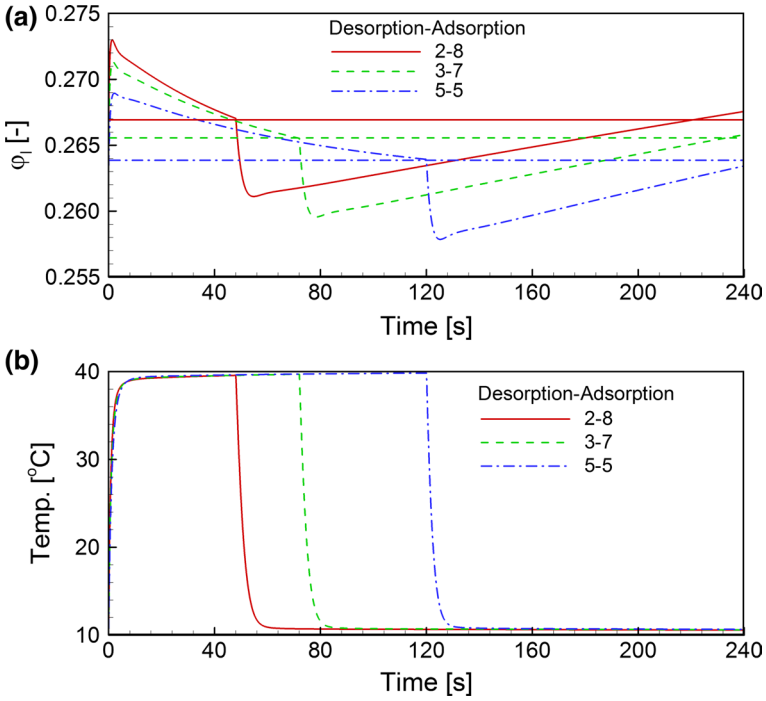

Fig. 12 Changes in **a** water mass fraction and **b** temperature in desiccant during single steady cycle for different D–A ratios (relative humidity of air = 40 %, air flow rate = 0.04 kg/s, and cycle period = 240 s)

function because the liquid water mass fraction at the end of desorption was less than that at the end of adsorption. The actual dehumidified amount was significantly lower than the hygrothermal surge. However, the dehumidified amount and surge can dramatically vary with the operating conditions. Technically it is important how to increase the dehumidified amount and at the same time how to decrease the hygrothermal surge.

3.3 Hygroscopic performance for various operating conditions

As shown in Fig. 11, we checked that the amount of dehumidified water during one cycle was not significant compared to the hygrothermal surge. The time for the desiccant's thermal development seemed slightly long compared to the time period for a single cycle. Thus, to check if the dehumidification performance can be effectively enhanced by regulating the operating conditions, we examined the effects of the D–A ratio, cycle period (rotor speed), and mass flow rate of the inflowing air.

3.3.1 Ratio of time periods for desorption and adsorption

First, we adjusted the ratio of the time periods for desorption and adsorption (D–A ratio) by adopting a simple mechanical device to divide the rotor in two segments: for the hot air from the condenser (for desorption) and for the cold air from the evaporator (for adsorption). D–A ratios of 2–8, 3–7, and 5–5 were tested for a cycle period of 240 s (0.25 rpm). The thermo-psychrometric conditions for the inflowing air in the desorption and adsorption processes were equal to those for the case described in Fig. 5. The flow rates of the humid air for desorption and adsorption were identical at 0.04 kg/s. As noted earlier, this was the mass flow rate for the entire rotor; thus, the mass flux should be recalculated considering the D–A ratio and rotor diameter of 0.2 m. The mass fluxes for desorption and adsorption thus had different values, unlike the mass flow rate. The vapor mass fraction of the inflowing air for desorption was 0.02 (relative humidity = 40 %), which was double the case shown in Fig. 5. The vapor mass fraction of the inflowing air for adsorption was 0.004.

Figure 12 shows the changes of the liquid water mass fraction and temperature in the desiccant for one steady cycle. Regulating the D–A ratio did not significantly increase the amount of dehumidified water. The amount of dehumidified water for one cycle still remained very small compared to the hygrothermal surge. However, we determined that the time for the rotor's thermal development is independent of the D–A ratio and cycle period. The horizontal lines in Fig. 12a are auxiliary lines that allow the differences between the liquid water mass fractions at the ends of desorption and adsorption to be easily checked. For the present case (40 % relative humidity of the air for desorption), the increasing the adsorption portion was favorable for dehumidification. The case of a 5–5 D–A ratio worked adversely, i.e., the rotor adsorbed vapor during the desorption period and desorbed vapor during the adsorption period. That is, having the cold air from the evaporator

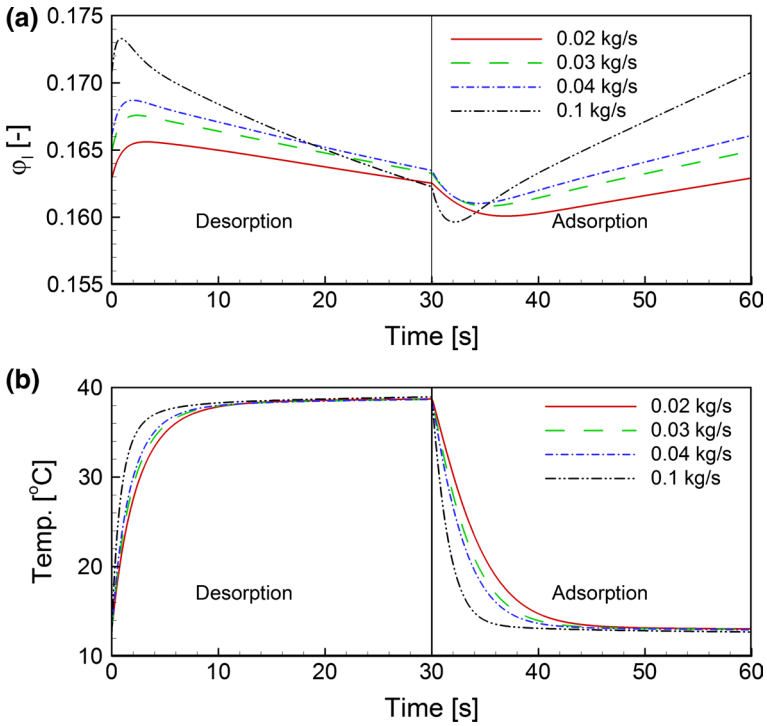

Fig. 13 Changes in **a** water mass fraction and **b** temperature in desiccant during single steady cycle for different air flow rates (relative humidity of air = 40 %, D–A ratio = 5–5, and cycle period = 60 s)

pass through the adsorption sector of the hygroscopic rotor is not helpful at all to achieve a much lower humidity of the air; having the cold air bypass on its way to the room or only part of the cold air pass through the rotor is more effective.

3.3.2 *Mass flow rate*

To check the effects of the air inflow rate, simulations were conducted for four different air inflow rates: 0.02, 0.03, 0.04 and 0.1 kg/s. The D–A ratio was fixed to 5–5, the cycle period was 60 s (1 rpm), and the temperatures and vapor mass fractions of the inflowing air for desorption and adsorption were equal to those given in Fig. 12.

As shown in Fig. 13, the dehumidification performance of the rotor gradually increased with the flow rate. The case with the largest flow rate of 0.1 kg/s reached a thermally developed state most rapidly because of its high thermal capacity, as shown in Fig. 13b. During the adsorption period, especially, this rapid thermal development made the rotor start practical vapor adsorption very early, as shown in Fig. 13a. In addition, the increased flow rate clearly produced a larger mass transfer potential between the flow and desiccant layer; as a result, the liquid water mass fraction in the desiccant decreased and increased much more during desorption and adsorption, respectively, as shown in Fig. 13a. Because of these effects, a larger amount of water was dehumidified when the air inflow rate was increased.

3.3.3 *Cycle period (rotor speed)*

The results in Fig. 12 makes us curious how the dehumidification performance varies when the absolute time for adsorption increases, because the figure showed that the dehumidification performance is apparently enhanced when the time for the adsorption period is increased. However, the regulating D–A ratio was limited. Thus, in this numerical simulation, we varied the cycle period from 60 s (rotor speed = 1 rpm) to 480 s (rotor speed = 0.125 rpm). For all cases, the D–A ratio was fixed to 2–8, the humid air inflow rates for desorption and adsorption were identical at 0.04 kg/s, and the temperatures and vapor mass fractions of the inflowing air for desorption and adsorption were equal to those for the cases in Figs. 12 and 13.

As shown in Fig. 14, the short cycle periods of 60 and 120 s had an adverse effect (i.e., the air was not dehumidified), and the cycle periods of 240 and 480 s produced a favorable dehumidification function. As expected, the dehumidification performance was definitely enhanced when the cycle period was increased. Figure 14 only shows the dehumidified water amount for a single cycle. However, although the amount of dehumidified water for a single cycle is increased by increasing the cycle period, the amount of dehumidified water normalized by unit time could not be increased. Thus, we needed to check whether increasing the cycle period is really effective by comparing the time-based dehumidification rate in the unit of [g/min].

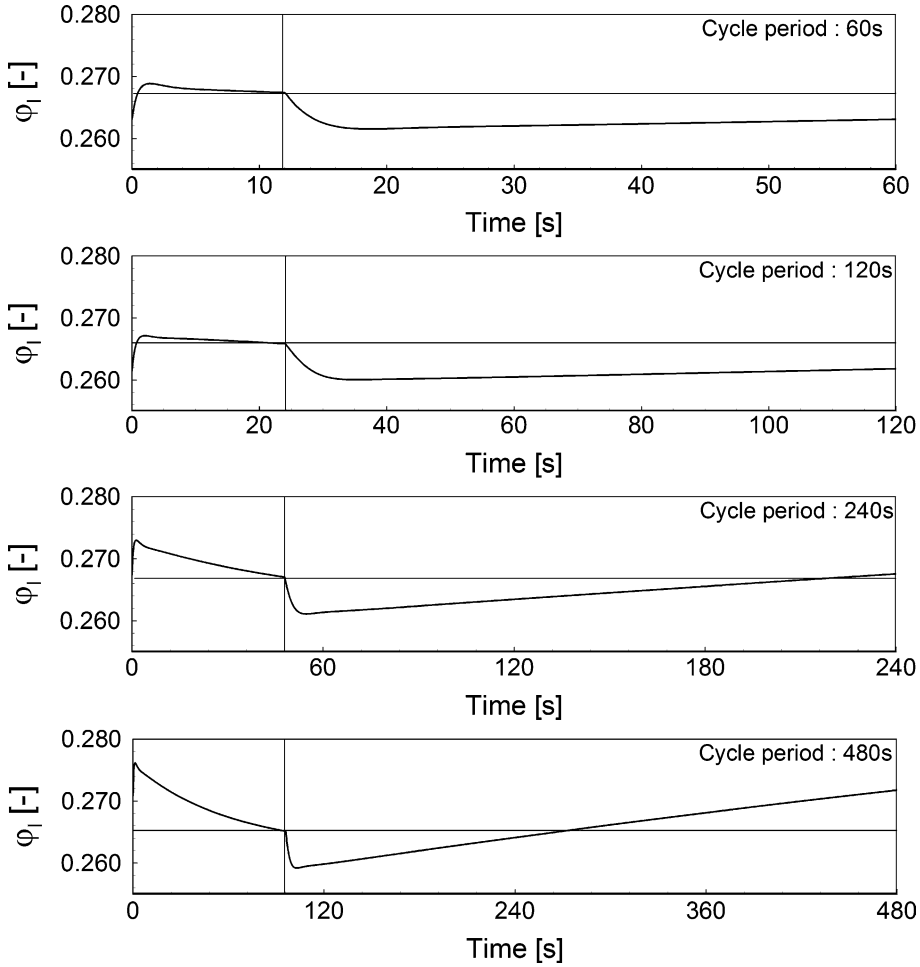

Fig. 14 Changes in water mass fraction and temperature in desiccant during single steady cycle for different cycle periods (relative humidity of air = 40 %, D–A ratio = 2–8, and air flow rate = 0.04 kg/s)

In addition, we needed to determine whether the dehumidification performance continuously increases with increasing cycle period.

Figure 15 compares the dehumidification rates for eight different cycle periods: 60, 120, 240, 360, 480, 600, 1200, and 1800 s. The dehumidification rate significantly increased with the cycle period up to 600 s. For the longer cycle periods, the dehumidification rate no longer increased with the cycle period, and the cycle period of 1800 s actually showed a slightly lower dehumidification rate than the cycle period of 1200 s.

3.4 Dehumidification performance for various working environments

We checked that the dehumidification performance of the hygroscopic rotor dramatically varies with changes in the operating conditions, such as the D–A ratio, air flow rate, and cycle period. Until now, we found that increasing the time for adsorption, the air flow rate, and the cycle period

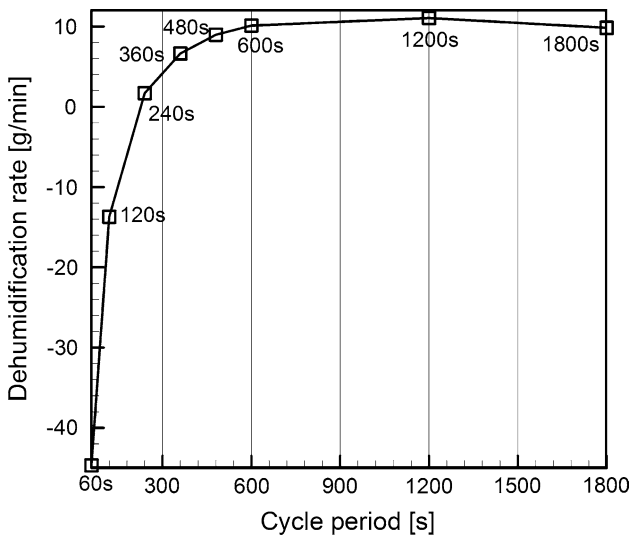

Fig. 15 Dehumidification rate depending on cycle period (relative humidity of air = 40 %, D–A ratio = 2–8, and air flow rate = 0.04 kg/s)

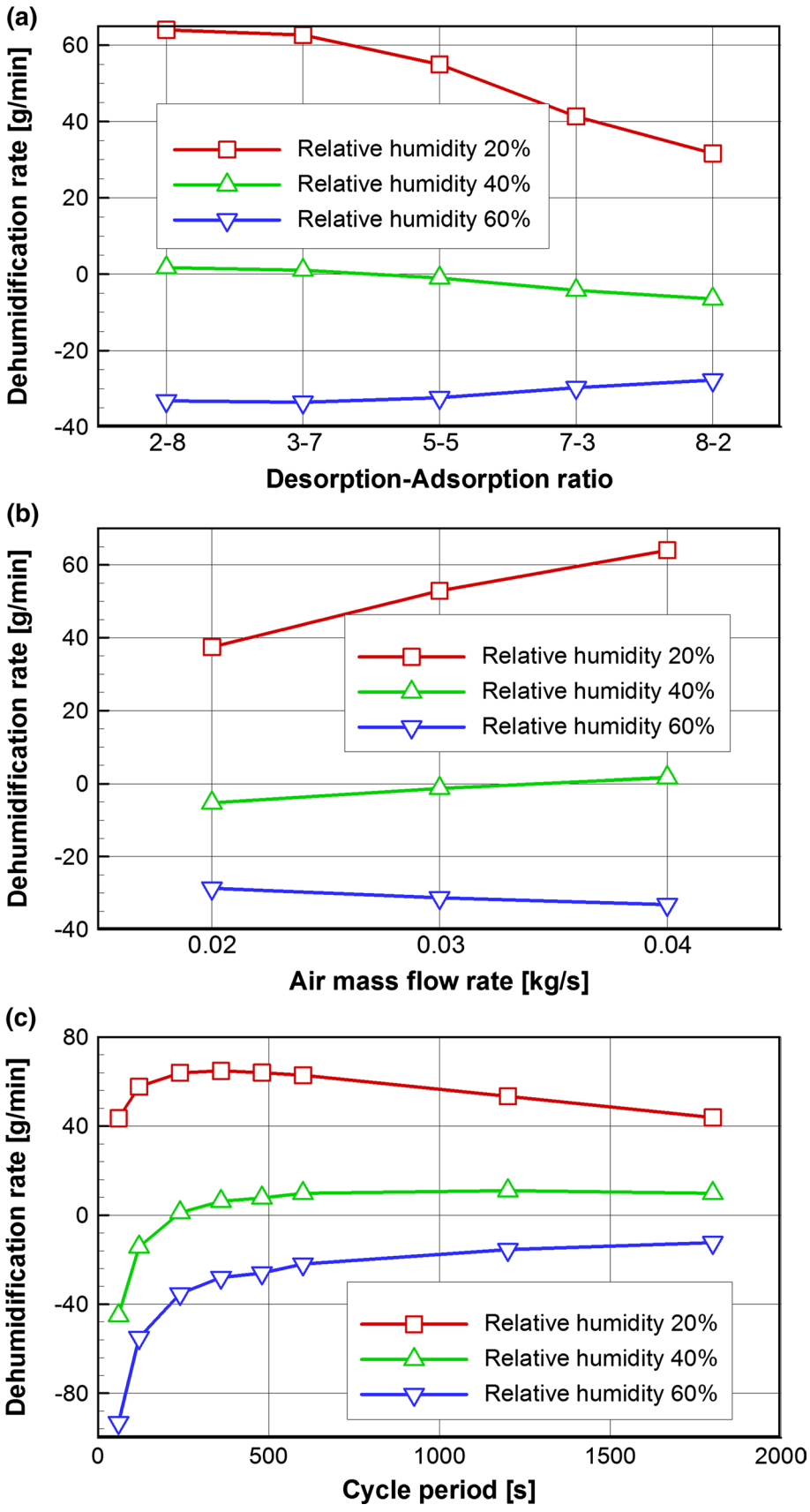

Fig. 16 Dehumidification rate for different air humidities depending on **a** D–A ratio, **b** air flow rate, and **c** cycle period

all helped with dehumidification. However, we needed to check if doing so would still apply in other working environments with different air humidities and temperatures. Thus, the simulations were continued for three different relative humidities of 20, 40, and 60 %. The desiccant's initial hygrothermal state and the inflowing air's thermal-psychrometric condition were equal to those for the cases described in Figs. 12, 13, and 14.

First, Fig. 16a shows the dehumidification rate along with the D–A ratio from 2–8 to 8–2 for the three different air humidity conditions. The air flow rate and cycle period were fixed to 0.04 kg/s and 240 s respectively. The pre-conclusion about the D–A ratio was only valid for relatively dry cases with a relative humidity of 20 and 40 %. When the relative humidity was 60 %, the dehumidification rate increased as the time portion for adsorption decreased. That is, in highly humid environments, dehumidification requires more time for desorption to regenerate the rotor. In any event, the highly humid case of 60 % relative humidity appears to require other remedies for correct functioning, such as changing the cycle period or incoming air temperature. As shown in Fig. 16a, adjusting the D–A ratio to enhance the dehumidification performance is meaningful only under very low humidity conditions, such as a relative humidity of 20 %.

Next, Fig. 16b presents the dehumidification rates for different air flow rates and relative humidities. The D–A ratio and cycle period were fixed to 2–8 and 240 s, respectively. Increasing the air flow rate was only favorable for the low humidity cases with relative humidities of 20 and 40 %. Increasing the air flow rate was originally expected to be favorable for dehumidification in all cases because of the enhancement in heat and mass transfer caused by its convection effects. However, in the high-humidity case of 60 %, the dehumidification rate decreased as the air flow rate increased; further, a negative dehumidification rate was detected for all the tested air flow rate conditions. This means that the highly wet (humid) air can negatively affect dehumidification by boosting the convection effect.

Figure 16c shows the changes in the dehumidification rate depending on the cycle period for the three different air humidity conditions. The D–A ratio and air flow rate were fixed to 2–8 and 0.04 kg/s, respectively. In Fig. 15, the dehumidification rate became saturated as the cycle period increased. Here, however, the dehumidification rate was maximized around the cycle period of 360 s at a low relative humidity of 20 %; it decreased with larger cycle periods. On the other hand, at a relative humidity of 60 %, the dehumidification rate was still increasing with increasing cycle period by 1800 s.

Based on the above results, the hygroscopic rotor does not work favorably under very humid conditions, such as a relative humidity of 60 %. All cases with a relative humidity of 60 % showed a negative dehumidification rate regardless of adjustment to the D–A ratio, air flow rate, and cycle period. Here, we investigated the effect of the inflowing air temperature. As noted earlier, the temperature of the air flowing into a hybrid dehumidifier can surely be regulated by adjusting the operation of the refrigerating part. Figure 17 shows the dehumidification rates for different inflowing air temperatures during the desorption period. The D–A ratio, air flow rate, and cycle period were fixed to 2–8, 0.04 kg/s, and 240 s, respectively. The air temperature for the adsorption period was fixed to 10 °C, just like in the previous cases. As shown in Fig. 17, regardless of the relative humidity, the dehumidification rate exponentially increased as the air temperature was increased for the desorption period. The case of a relative humidity of 60 % for the first time showed a favorable dehumidification function for the 50 °C incoming air for desorption. Increasing the inflowing air temperature for desorption is highly effective for enhancing the dehumidification performance; the case of 20 % and 50 °C showed a dehumidification rate over 100 g/min. This is a quite meaningful achievement, keeping in mind that all the other operating parameters could enhance the dehumidification rate to only 60 or 70 g/min.

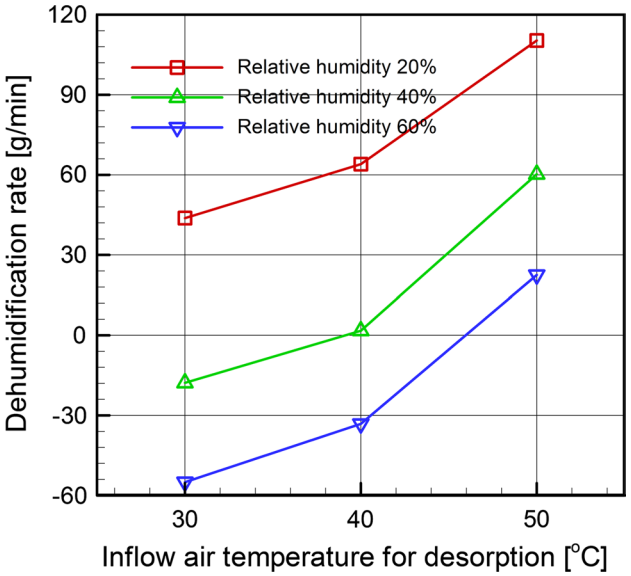

Fig. 17 Dehumidification rate for different air humidities depending on inflowing air temperature for desorption period

A greater difference between the inflowing air temperatures for the adsorption and desorption periods allowed for larger working ranges in the vapor mass fraction and liquid water mass fraction in the desiccant, as shown in the desiccant's hygrothermal map of Fig. 10. Of course, generating a larger difference in air temperatures for the adsorption and desorption periods would require more energy consumption for the operation of the refrigerating cycle. Thus, shifting the

working temperature range according to the given air conditions would be favorable for enhancing the hybrid effects.

4 Conclusions

The heat and mass transfers in a hygroscopic rotor were numerically investigated based on a two-dimensional model for the conjugate transports between the flow and desiccant layers. The silica gel RD was used as the desiccant material, while the Knudsen diffusion was ignored. A conjugation procedure that included the heat and mass sources in both the flow and desiccant layers was set up. By the developed conjugation procedure, the details of the minute changes in temperature, vapor mass fraction, and liquid water mass fraction in the early stages of desorption and adsorption period during the consecutive cycles, were physically-well explained. Especially, the hygrothermal surging phenomenon in the desiccant was successfully reproduced in the present unsteady sorption simulation. For the consecutive sorption cycles, the desiccant's hygrothermal state was tracked on the present desiccant's hygrothermal map. By mapping the rotor's hygrothermal state, the complex sorption processes could be more understandable. The variation in the dehumidification performance was investigated by regulating the rotor operating conditions for various working environments with regard to the air humidity and temperature.

It was revealed that the D–A ratio meaningfully influences the dehumidification performance under only very low humidity conditions. For highly humid conditions, increasing the air flow rate can negatively affect dehumidification. As the air humidity increases, the optimal cycle period increases. It was found that increasing the air temperature for desorption tremendously enhanced the dehumidification. In a hybrid dehumidifier, the regulating the incoming air temperature through operation of the refrigerating part is essential to increasing the contribution of the hygroscopic part.

Acknowledgments This subject is supported by Ministry of Environment as "Eco-innovation".

References

1. Sphaier LA, Worek WM (2004) Analysis of heat and mass transfer in porous sorbents used in rotary regenerators. Int J Heat Mass Transf 47(14–16):3415–3430
2. Zhang LZ, Niu JL (2002) Performance comparisons of desiccant wheels for air dehumidification and enthalpy recovery. Appl Therm Eng 22(12):1347–1367
3. Ruivo CR, Costa JJ, Figueiredo AR (2007) On the behavior of hygroscopic wheels: part I-channel modelling. Int J Heat Mass Transf 50:4812–4822
4. Ghali K, Othmani M, Ghaddar N (2008) Energy consumption and feasibility study of a hybrid desiccant dehumidification air conditioning system in Beirut. Int J Green Energy 5(5):360–372
5. Jeong J, Yamaguchi S, Saito K, Kawai S (2010) Performance analysis of four-partition desiccant wheel and hybrid dehumidification air-conditioning system. Int J Refrig 33(3):496–509
6. Brillhart PL (1997) Evaluation of desiccant rotor matrices using an advanced fixed-bed test system, PhD thesis, University of Illinois at Chicago
7. Simonson C, Besant R (1997) Heat and moisture transfer in desiccant coated rotary energy exchangers: part I. Numerical model. HVAC&R Research 3(4):325–350
8. Simonson C, Besant R (1997) Heat and moisture transfer in desiccant coated rotary energy exchangers: part II. Validation and sensitivity studies. HVAC&R Research 3(4):351–368
9. Pesaran AA (1983) Moisture transport in silica particle beds, PhD thesis, University of California, Los Angels
10. Majumdar P (1998) Heat and mass transfer in composite desiccant pore structures for dehumidification. Sol Energy 62(1):1–10
11. Dai YJ, Wang RZ, Zhang HF (2001) Parameter analysis to improve rotary desiccant dehumidification using a mathematical model. Int J Therm Sci 40(4):400–408
12. Golubovic MN, Worek WM (2004) Influence of elevated pressure on sorption in desiccant wheels. Numer Heat Tranf Part A: Appl: Int J Comput Methodol 45(9):869–886
13. Ni C-C, San J-Y (2000) Mass diffusion in a spherical microporous particle with thermal effect and gas-side mass transfer resistance. Int J Heat Mass Transf 43(12):2129–2139
14. Zhang XJ, Dai YJ, Wang RZ (2003) A simulation study of heat and mass transfer in a honeycombed rotary desiccant dehumidifier. Appl Therm Eng 23(8):989–1003
15. Ruivo CR, Costa JJ, Figueiredo AR (2006) Analysis of simplifying assumptions for the numerical modeling of the heat and mass transfer in a porous desiccant medium. Numer Heat Tranf Part A: Appl: Int J Comput Methodol 49(9):851–872
16. Ruivo CR, Costa JJ, Figueiredo AR (2008) On the validity of lumped capacitance approaches for the numerical prediction of heat and mass transfer in desiccant airflow systems. Int J Therm Sci 47(3):282–292
17. San JY, Hsiau SC (1993) Effect of axial solid heat conduction and mass diffusion in a rotary heat and mass regenerator. Int J Heat Mass Transf 36(8):2051–2059
18. Fujii Y, Lior N (1996) Conjugate heat and mass transfer in a desiccant-airflow system: a numerical solution method. Numer Heat Tranf Part A: Appl: Int J Comput Methodol 29(7):689–706
19. Al-Sharqawl HS, Lior N (2004) Conjugate computation of transient flow and heat and mass transfer between humid air and desiccant plates and channels. Numer Heat Tranf Part A: Appl: Int J Comput Methodol 46(6):525–548
20. Sherony DF, Solbrig CW (1970) Analytical investigation of heat or mass transfer and friction factors in a corrugated duct heat or mass exchanger. Int J Heat Mass Transf 13(1):145–159
21. Gao Z, Mei VC, Tomlinson JJ (2005) Theoretical analysis of dehumidification process in a desiccant wheel. Heat Mass Transf 41(11):1033–1042
22. Sphaier LA, Worek WM (2006) Comparisons between 2-D and 1-D formulations of heat and mass transfer in rotary regenerators. Numer Heat Transf Part B: Fundam: Int J Comput Methodol 49(3):223–237